J. Synchrotron Rad. (1995). **2**, 124–131

A Double Multilayer Monochromator at an ESRF Undulator for Microbeam Experiments

P. Deschamps, P. Engström, S. Fiedler, C. Riekel,* S. Wakatsuki, P. Høghøj† and E. Ziegler

European Synchrotron Radiation Facility, BP 220, F-38043 Grenoble CEDEX, France

(*Received 19 September 1994; accepted 1 February 1995*)

A water-cooled double W/Si-multilayer monochromator has been operated at an ESRF low-β undulator beam. For a fixed distance of the two multilayers the first-order Bragg reflection was at ~8 keV. The peak power density of the beam at the exit of the multilayers was ~1 W mm^{-2} and the flux density of the first order after a 10 μm collimator was 4 × 10^5 photons s^{-1} μm^{-2} mA^{-1}. The performance of the beam in microbeam diffraction has been tested on a 20 μm W wire. The observed pseudo-Laue pattern is discussed with respect to the multilayer spectrum.

Keywords: multilayer monochromator; microbeams; undulators; microdiffraction; Laue diffraction.

1. Introduction

Multilayer optics are of interest for hard X-ray synchrotron radiation experiments as broad bandpass monochromators. Applications in time-resolved small-angle X-ray scattering (SAXS) (Stephenson, 1988), powder diffraction (Pennartz, Löchner, Fuess & Wroblewski, 1992) and microfluorescence (Underwood, Thompson, Wu & Giauque, 1988) have been reported.

The use of multilayers at undulator beamlines of third-generation synchrotron radiation sources is interesting as the bandwidth of the undulator peaks roughly matches the bandwidth of the multilayer peaks. Undulator harmonics are polluted by side bands due to other harmonics. This is particularly so for low-β undulators when the divergence does not allow the central cone to be separated from the rest of the spectrum. The use of multilayers should allow filtering of the spectrum, which is of interest where the narrow bandwidth provided by a perfect crystal monochromator is not of prime importance, but instead a high flux density is required.

The present paper reports on a double multilayer monochromator developed for the microfocus beamline at the European Synchrotron Radiation Facility (ESRF). The applications of this monochromator will be principally in micro-diffraction and micro-diffuse scattering experiments (Riekel, 1993). The main aim has been to reach a maximum throughput at a selected wavelength. The present multilayers have been optimized for 8 keV.

2. Source parameters

The ESRF is a third-generation high-brilliance source (ESRF, 1994). For the present experiments the low-β undulator of the microfocus beamline was used (Riekel, 1993). The source parameters are given in Tables 1 and 2.

3. Optical system

A schematic diagram of the optics of the microfocus beamline (Riekel, 1993; Engström, Fiedler & Riekel, 1995) is shown in Fig. 1. The beam reflected from the first multilayer crystal passes through the channel of a channel-cut Si(111) crystal. The second multilayer crystal is at a fixed distance of 1352 mm from the first crystal. The focusing ellipsoidal mirror at a distance of 31 m from the source was not used in these studies. A 10 μm collimator could be inserted into the beam path for microbeam experiments. In order to be able to select several wavelengths, different multilayer periods are necessary. For the present application, W/Si multilayers with the first-order Bragg reflection at ~8 keV were used. The optimum period for the multilayers was calculated based on the Fresnel formalism [Høghøj, Ziegler & Riekel, 1992; original software code from Brennan (1990)].

Multilayers were produced on a custom-order basis (Ovonics Synthetic Materials Corporation). Si single-crystal

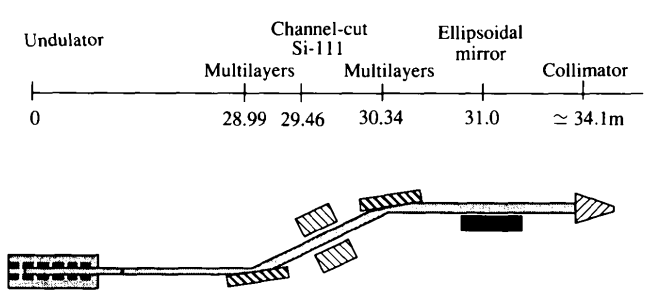

Figure 1
Schematic layout of the microfocus beamline optics (Riekel, 1993). The horizontal distance between the multilayers is 1352 mm, the beam offset in the vertical plane is 20 mm.

* Author to whom correspondence should be addressed.
† Present address: Institut Max von Laue–Paul Langevin, BP 156X, F-38042 Grenoble CEDEX, France.

© 1995 International Union of Crystallography
Printed in Great Britain – all rights reserved

Table 1
Microfocus beamline undulator properties.

Spectral flux [photons s^{-1} (0.1% bandwidth)$^{-1}$]	Spectral brilliance [photons s^{-1} mm^{-2} $mrad^{-2}$ (0.1% bandwidth)$^{-1}$]	l_u (mm)	Length (mm)	Power (kW)	E_c (keV)	B (T)	K
7×10^{13}	1.4×10^{17}	46	1518	0.1	11.6	≤ 0.52	≤ 2.2

Notes: current, 100 mA; magnetic gap, ≥ 20 mm; l_u, undulator period; E_c, critical energy; B, magnetic field.

Table 2
Photon source dimensions of the low-β undulator.

x_s (mm)	z_s (mm)	x_s' (mrad)	z_s' (mrad)
0.133	0.088	0.230	0.042

Notes: x_s, x_s' correspond to the horizontal; z_s, z_s' to the vertical directions (FWHM).

substrates of dimensions 150 (l) × 20 (w) × 10 mm (t) were used. The Si substrates were shaped by A. Paul of the ESRF optics group. The Si surfaces were polished (Melles-Griot and General Optics) to a surface roughness of ~3 Å and a slope error of ~1 arcsec. 30 bilayers were deposited for the multilayer with a period of 132 Å (d_W = 13, d_{Si} = 119 Å). This results in a fundamental at 8 keV at a reflection angle of $\theta = 0.42°$. The system has, however, enough mechanical freedom that the first order can be varied in the range 8–9 keV. The smaller power density as compared to an Si monochromator allows water cooling to be used (Ziegler *et al.*, 1992).

A reflectivity of ~80% for the first-order Bragg reflection was derived from laboratory angular dispersive experiments (Høghøj *et al.*, 1994). The d-spacing variation of the first order at selected points across the whole surface was ~0.9% and the $\Delta E/E$ of the first order was 0.17 (FWHM).

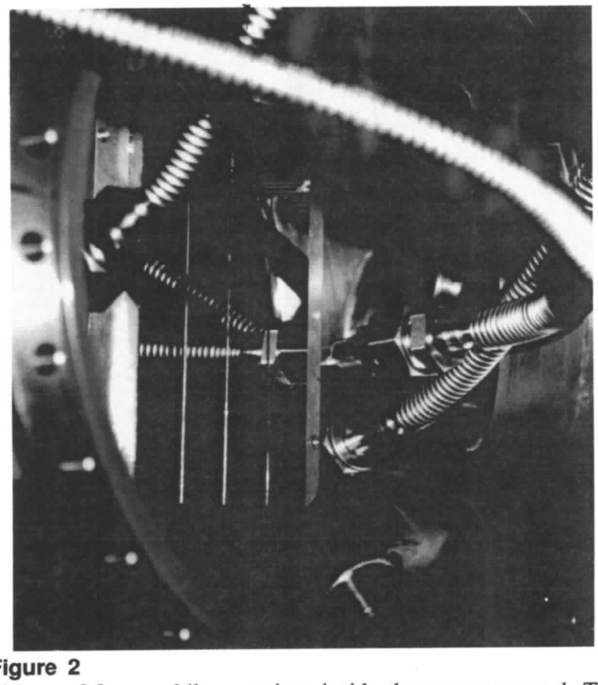

Figure 2
Picture of four multilayer stripes inside the vacuum vessel. The water-cooled copper support is visible.

The multilayers were installed in separate vacuum chambers (GMI Grenoble) with the possibility of angular rotation (θ), upward translation and lateral selection of individual stripes of multilayers by stepper motors. The set-up allows up to four different multilayer stripes to be translated into the beam. The substrates were fixed on a water-cooled copper support. Thermal contact was achieved by use of In/Ga alloy. Fig. 2 shows an image of four stripes inside the vacuum chamber. Both vacuum chambers were ion pumped to ~10^{-7} mbar.

4. Simulation

Ray-tracing with the *SHADOW* code (Cerrina & Lai, 1986) was performed in order to simulate the spectra. The calculated spectrum of the multilayers (150 bilayers) is shown in Fig. 3(*a*). Fig. 3(*b*) shows the calculated undulator spectrum for a gap of 22.5 mm (K = 1.904) including filters of 0.26 mm carbon and 1 mm Be windows corresponding to the microfocus beamline. The calculated folded spectrum is shown in Fig. 3(*c*). Note that the range of total reflection is almost completely suppressed due to the filters used.

The calculated influence of a variation of the undulator gap on the transmitted flux is shown in Fig. 4. Optimum throughput is obtained when the energy of the third undulator harmonic matches the energy of the multilayer peak at a gap of 22.5 mm (K = 1.90). The asymmetry of the peak is due to the larger bandwidth of the multilayers as compared to the undulator third harmonic. An increase in gap results in a shift of the undulator harmonics to higher energies. Thus, at 24.2 mm the bump at the lower energy side of the third harmonic will fall into the acceptance window of the multilayers and at 29.9 mm gap this will be the case for the second undulator harmonic. These calculations show that the selected gap, and hence the position of the undulator third harmonic, will considerably modify the transmitted multilayer fundamental. Furthermore, the choice of optimization of throughput on the undulator third harmonic implies that the other undulator harmonics will not be transmitted with a high efficiency due to the different periodicity of the undulator and multilayer spectra.

5. Experimental results

5.1. *Spectrum, power output and stability*

For alignment, rocking curve scans were performed for a gap of ~21 mm. The flux was recorded by a photo-

diode. High-resolution topography of the transmitted beam recorded on Kodak film shows strong intensity modulations (Fig. 5). The origin might be due to growth irregularities of the multilayers – rather than the substrate surface in view of its perfection and/or irregularities in the upstream Be window.

For flux optimization an undulator gap scan was performed and the air scattered spectrum recorded by a Ge detector at 90°. For analysis, a ΔE window at the first (Fig. 6*a*) and the second multilayer order (Fig. 6*b*) was chosen. The observed maxima correspond to the successive undulator harmonics passing through the window as the

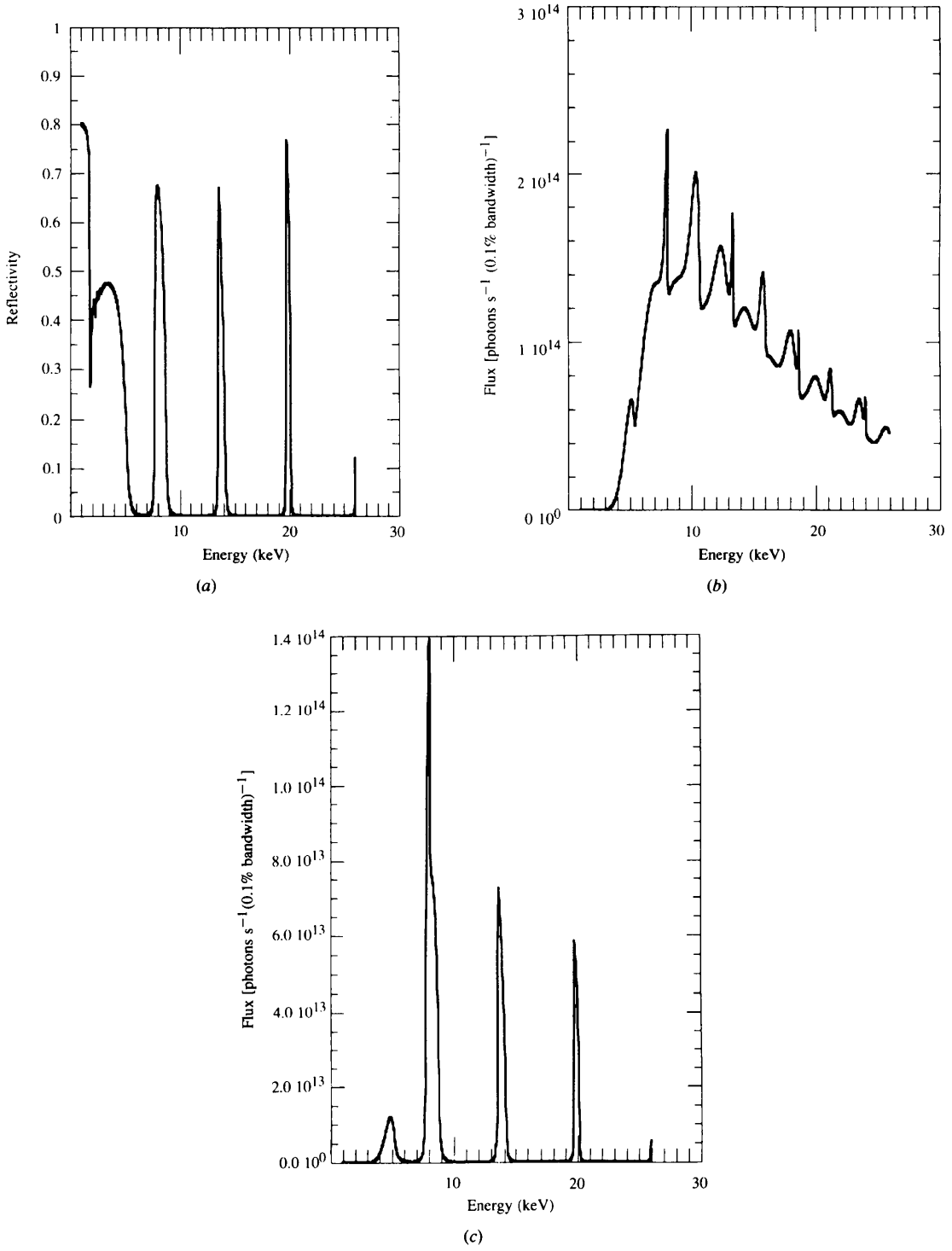

Figure 3
(*a*) Reflectivity of multilayers without roughness (period: see §3) calculated by *SHADOW*. (*b*) Calculated flux of the microfocus beamline undulator for a gap of 22.5 mm (K = 1.904) including absorption due to the 0.26 mm carbon filter and 1 mm Be window; full beam. (*c*) Calculated flux for folded spectra of (*a*) and (*b*). Undulator gap: 22.5 mm (K = 1.904); full beam.

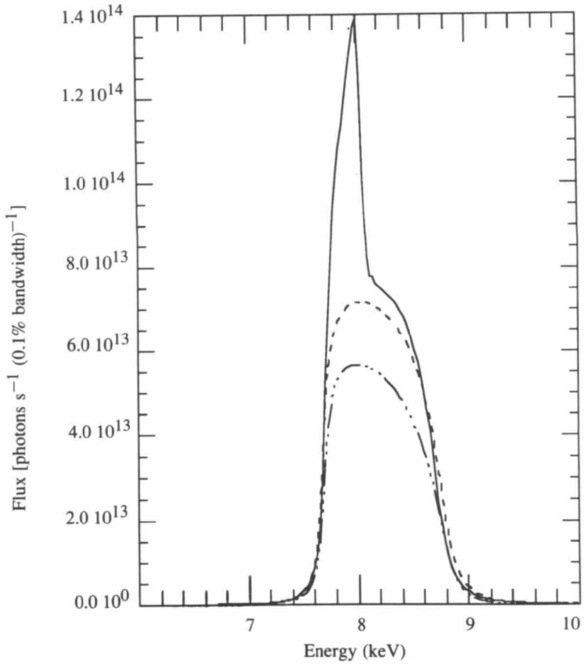

Figure 4
Influence of undulator gap on transmitted flux at the multilayer first-order Bragg reflection. Parts of the undulator spectrum falling into the acceptance window of multilayers: — third harmonic (22.5 mm gap; K = 1.9); – – – bump at smaller energy as third harmonics (24.2 mm gap; K = 1.7); –·–·– second harmonic (29.9 mm gap; K = 1.2).

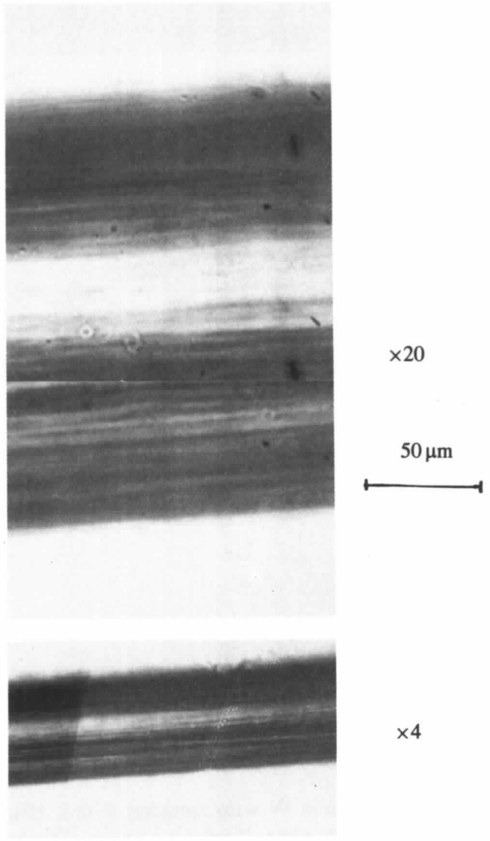

Figure 5
Topography of the beam after the double multilayer system by high-resolution film. The magnification of the film is indicated.

gap is changed. For further experiments a gap of 23 mm was chosen corresponding to the third undulator harmonic matching the multilayer first order. This gap is close, although not exactly equal to the ideal gap settings indicated in Fig. 4 and suggests a slight detuning of the multilayer crystals. The full undulator spectrum, recorded at a gap of 23 mm (Fig. 7), is in reasonable agreement with the calculated spectrum (Fig. 3*c*). The spectrum is mainly due to inelastic scattering. Note that the resolution function of the Ge detector results in a broadening of the third harmonic.

The power output of the multilayer beam was measured by a Cu calorimeter. A peak power density of $\sim$1 W mm^{-2} was determined. The flux of the first five orders was determined by the Ge detector after the 10 μm collimator (beam size 7 μm FWHM after collimation) with calibrated metal foils (*e.g.* Fe for the first order; see Table 3). The flux density of the first order of $\sim 4 \times 10^5$ photons s^{-1} μm^{-2} mA^{-1}

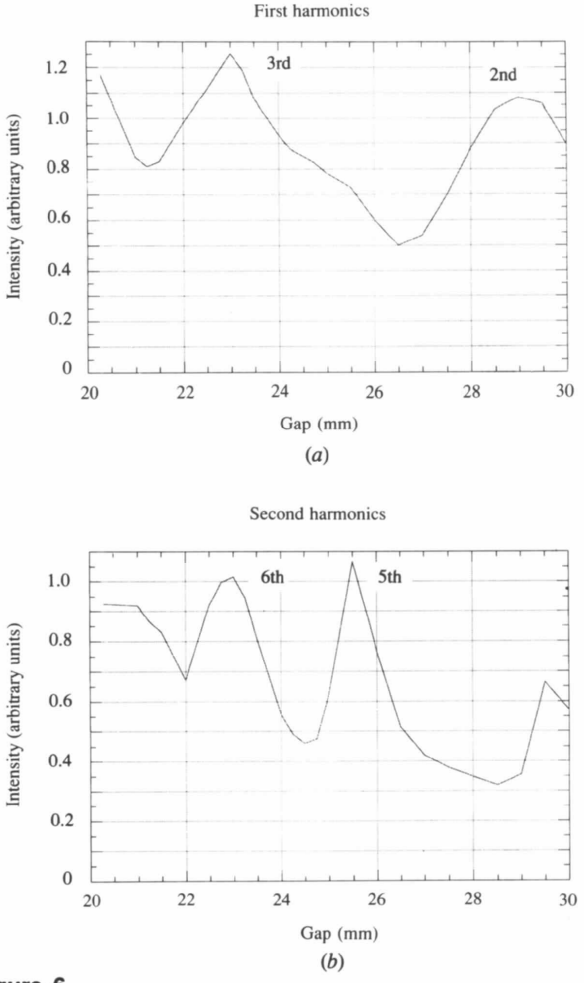

Figure 6
Undulator gap scan. The intensity corresponds to the multilayer first-order Bragg reflection recorded by a Ge detector. (*a*) The maxima correspond to the undulator third and second harmonics matching the multilayer first order. (*b*) Match of second-order Bragg reflections of multilayers for the undulator sixth and fifth harmonics. Note the larger width of the even order.

Table 3
Flux for the first five orders determined by a Ge detector at 100 mA and after the 10 μm collimator.

Order	Flux (photons s^{-1})
1	6×10^9
2	1×10^9
3	9×10^8
4	8×10^8
5	8×10^7

is more than two orders of magnitude higher than the flux density reached with the same collimator after an Si(111) monochromator on the microfocus beamline (Engström *et al.*, 1995). A comparison of beam sizes and flux densities reached with various multilayer experiments is made in Table 4. In general, the present optics reaches flux density values similar to those obtained with focusing optics at bending-magnet sources. The highest flux density has been reported for Kirkpatrick–Baez multilayer mirrors at the CHESS undulator (Thompson *et al.*, 1992). Extrapolation from the monochromatic flux-density enhancement of the recently installed ellipsoidal mirror at the microfocus beamline (Engström *et al.*, 1995) suggests that it should be possible to increase the flux density of the multilayer first order of the microfocus beamline by a factor of $\sim 4 \times 10^4$. The focal spot size of such a beam could be reduced to $1 \times 1\,\mu m^2$ by a post collimator while still retaining a flux of $\sim 2 \times 10^{12}$ photons s^{-1} at 100 mA. Such optics may be of particular interest for scanning microfluorescence experiments on weak scatterers provided that the heat load on the sample does not pose problems.

The double monochromator system has been used for several weeks without visible degradation of the spectrum. Deposition of carbon on the footprint of the beam was observed without affecting reflectivity and surface rough-

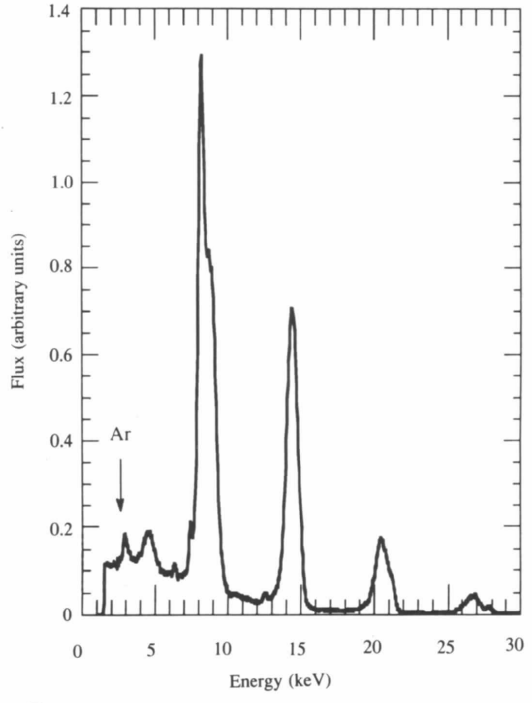

Figure 7
Spectrum of multilayers recorded by a Ge detector. Fluorescence peak due to Ar at ~3 keV and Ge-escape peak at ~5 keV.

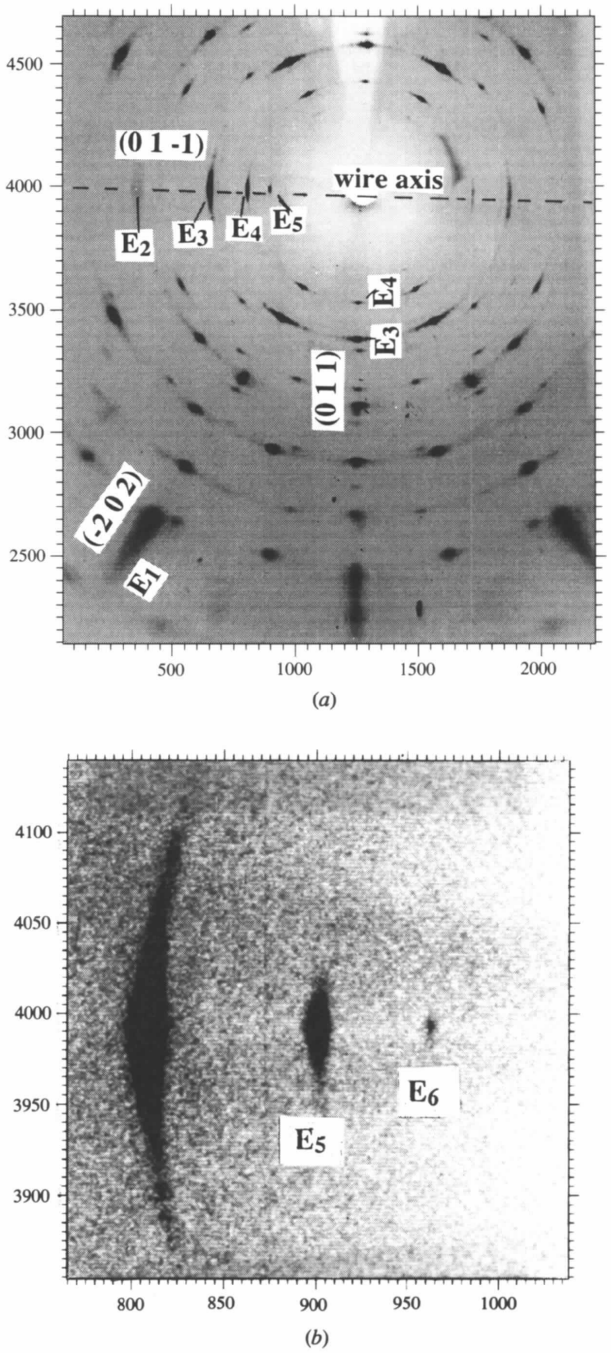

Figure 8
(*a*) Laue pattern of 20 mm W wire recorded with a 10 μm collimated beam on an image plate. Pixel size: 88 μm. The harmonics of the (011) and (01–1) reflections are indicated (symmetry-equivalent reflections are omitted). (*b*) A weak sixth harmonic of the (01–1) reflection is visible.

Table 4
Focal spot sizes (or smallest beam size at sample position) and flux densities reached for selected multilayer experiments.

Optics	Focal spot ($\mu m \times \mu m$)	Flux density [photons $s^{-1}\ \mu m^{-2}\ mA^{-1}$]	Bandwidth $\Delta E/E$	Source	Reference
Double multilayers*	157	4×10^5 (first orders)	1.7×10^{-1} at 8 keV	ESRF–UND	This article
BF multilayers†	5×2.5	1.6×10^6	$\sim 10^{-2}$ at 8 keV	ESRF–UND	Chevalier *et al.* (1995)
KB multilayer mirrors	4×9	3.6×10^8	2.6×10^{-2} at 8.6 keV	CHESS–UND	Thompson *et al.* (1992)
KB multilayer mirrors	6×8	2×10^5	$<10^{-1}$ at 10 keV	NLS–BM	Wu *et al.* (1990)
Double multilayers/mirror	$10^3 \times 10^3$	1×10^5	1.1×10^{-2} at 6 keV	NLS–BM	Stephenson (1988)
Single multilayers/mirror	$10^3 \times (3 \times 10^3)$	5×10^1	1.4×10^{-2} at 9.5 keV	DORIS–BM	Pennartz *et al.* (1992)

* Unfocused; after 10 μm collimator. † Abbreviations used: BF, Bragg–Fresnel; KB, Kirkpatrick–Baez; UND, undulator; BM, bending magnet.

ness. The glass window of the upstream multilayer chamber showed a brownish colour, presumably due to the formation of defects due to Compton scattering.

The present experiments were performed at a heat load of ~200 W and a heat density of ~0.2 W mm^{-2} (at θ = 0.42°). As a result of an increase of the ESRF ring current to 200 mA and a reduction of the emittance the heat load will increase to ~450 W and the heat density to ~0.5 W mm^{-2} for the same undulator gaps chosen in the present study. Whether the present cooling scheme is still sufficient under these conditions will have to be explored.

5.2. *Micro-diffraction on a metal wire*

In order to test the quality of the multilayer beam for micro-diffraction, experiments on a 20 μm thick W wire were performed with a first order set at 8.9 keV. Spectra were recorded on a BAS-UR (blue) FUJI image plate of 40 × 20 cm^2 size. The distance of the wire center to the plate was ~205 mm. Readout was performed with a Molecular Dynamics image-plate reader with a pixel size of 88 × 88 μm^2.

The 10 s pattern shows a wire texture with well defined reflections [Fig. 8(*a*); program *FIT2D* (A. Hammersley, ESRF)]. The wire axis is not exactly normal to the beam axis which explains the intensity asymmetry of the meridional reflections. The (011) and (01–1) reflections of the body-centered W lattice correspond to the multilayer orders E_2 = 15.0, E_3 = 21.5, E_4 = 28.3, E_5 = 35.1 keV, as indicated in Fig. 8. The first order is outside the recording range. The indexation suggests that the (011) plane is normal to the wire axis. This is expected for a freely drawn W wire (Kaelble, 1967). A careful analysis reveals evidence for a weak sixth harmonic of the (01–1) reflection at E_6 = 41.5 keV (Fig. 8*b*).

It is useful to discuss the interpretation of such spectra in more detail in view of potential applications in microcrystal Laue diffraction (Andrews, Hails, Harding & Cruickshank, 1987). Most of the spots have a broad distribution of 2–5° FWHM in the tangential direction, while the radial distribution of these spots is sharper. In principle, it should be possible to get more information on the crystallite distribution from these data. This is complicated – especially in the radial direction – by reflection asymmetries resulting from the uneven matching of undulator and multilayer harmonics, and is particularly evident for lower-order reflection harmonics such as the E_1 harmonic of the (–2,0,2) reflection.

The calculation of the crystallite distribution η(FWHM) from the spot shapes on the detector based on a polychromatic beam (Andrews *et al.*, 1987) does not apply in the present case since the wavelength distribution from the multilayers is rather limited. On the other hand, the summation of Gaussian distributions from different sources (Rosenbaum & Holmes, 1980) is not straightforward because of wide non-Gaussian profiles from wavelength distributions along the radial direction.

A mosaic distribution of ~5° (FWHM) implies that the spots would be very streaky in a pure polychromatic beam. In a semi-polychromatic beam, however, only those crystallites whose misorientation angle corresponds to the

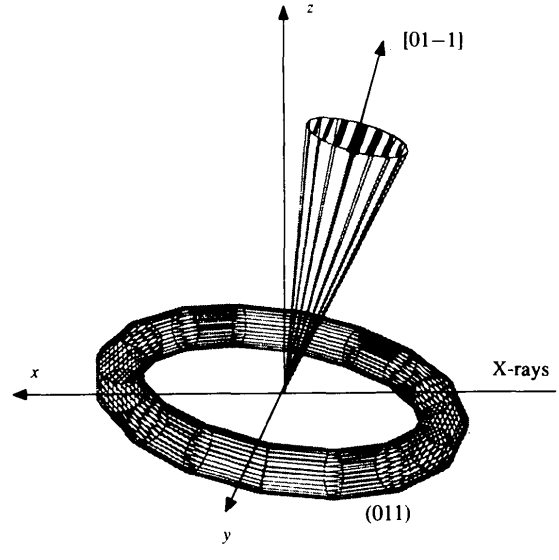

Figure 9
Schematic explanation of the origin of peak broadening in reciprocal space. The crystallite distribution of the (01–1) reflection is sampled by the different multilayer orders. A random orientation is present in an orthogonal plane for the (011) reflection.

wavelength of the multilayer spectrum can diffract. In this case one can map the detector position to wavelength for each reflection and estimate roughly the bandwidth of the spectrum. An example of such a calculation on the meridional (011) reflection is shown below:

E_2	14.6–15.4 keV
E_3	21.1–21.9 keV
E_4	27.9–28.7 keV
E_5	34.6–35.6 keV

The distribution of the crystallites in the W wire can be treated as in fibre diffraction. The [01–1] direction of each crystallite is oriented roughly along the wire axis with random orientation around the wire axis. The distribution of the [01–1] direction around the wire axis can be written as $P(\theta)$ where θ is the angle between wire axis and [01–1] direction (Fig. 9). The smearing of the meridional reflections forms a cap shape in reciprocal space which is sampled by the multilayer harmonics. The observed width in the tangential direction therefore arises directly from the shape of the cap with a maximal extension at the E_3 order.

The corresponding equatorial reflections in wire diffraction have a wide band generated by rotating similar caps, (011) and (01–1), about the wire axis (Fig. 9). This additional rotation sharpens the intensity distribution in the tangential direction. Each crystallite misoriented by θ_0 from the wire axis contributes to the intensity of the equatorial reflection at an angle θ' from the equatorial plane. The contribution from the crystallite-width misorientation θ_0 is only between 0 and θ_0. In other words, the intensity distribution of an equatorial reflection at an angle θ' is the summation of contributions from all crystallites with higher than θ' misorientation from the wire axis:

$$Q(\theta') = \int_{\theta'}^{\pi/2} P(\theta_0)\,\mathrm{d}\theta_0.$$

If one assumes a Gaussian distribution of the crystallites along the wire direction $P(\theta) = \exp(-\theta^2/2a)$, *i.e.* FWHM = $2.36a$, then the radial distribution of an equatorial reflection, *e.g.* (011), has the form of the error function

$$Q(\theta') = \int_{\theta'}^{\pi/2} \exp\left(-\theta^2/a^2\right)\mathrm{d}\theta \cong \int_{\theta'}^{\infty} \exp\left(-\theta^2/a^2\right)\mathrm{d}\theta$$

whose FWHM is $1.34a$. This explains why the equatorial reflections have narrower tangential distributions (~5° FWHM) than the largest meridional distribution, about 10° FWHM. Similar calculations can be applied to reflections which are not equatorial or meridional.

6. Summary

Stable operation of a water-cooled double multilayer monochromator at an undulator beam has been demonstrated. The high flux density should be of interest for a number of applications where a small beam in the range 1–10 μm with a moderately large bandwidth is required. For example, the low divergence of the undulator beam suggests applications in SAXS. The flux in a 7 μm FWHM collimated beam is already 6×10^9 photons s^{-1} at 100 mA and is expected to increase to $>1.2 \times 10^{10}$ photons s^{-1} at 200 mA. This value is close to the 1.5×10^{10} photons s^{-1} used for powder diffraction in the microsecond range at DORIS (Pennartz *et al.*, 1992) and suggests that dynamic structural processes could be studied at length scales in the range of a few micrometers with similar time resolution.

For applications in Laue diffraction the use of multilayer beams is advantageous in order to reduce the harmonics overlap present in polychromatic radiation (Glover & Helliwell, 1990). In contrast to monochromatic applications a smooth intensity distribution on the harmonics is required for wavelength normalization (Moffat, Kuriyan, Gilbert, Ringe & Karplus, 1986). In order to maintain the brilliance over the spectrum a better match of multilayers to undulator spectrum will be required.

For a number of applications the higher orders must be suppressed either by designing the multilayers correspondingly or by using mirror optics. For the ellipsoidal mirror of the microfocus beamline this has not been attempted in view of the unknown behavior of its Rh-covered Zerodur substrate in the multilayer beam. Alternatively, glass-capillary optics could be used (Thiel, Bilderback & Lewis, 1992; Hoffman, Thiel & Bilderback, 1992; Engström *et al.*, 1991).

We wish to thank J. Wood (Ovonics) for his continuous and efficient support. M. Lorenzen made helpful suggestions for the interpretation of the calorimetric data. The crystals were mounted by P. Wattecamps and M. Rossat. J. Gorini provided electronics support. I. Snigireva helped with photographic work. We are grateful to FUJI Film Co. Ltd for providing the blue image plates.

References

Andrews, S. J., Hails, J. E., Harding, M. M. & Cruickshank, D. E. J. (1987). *Acta Cryst.* A**43**, 70–73.
Brennan, S. M. (1990). Personal communication.
Cerrina, F. & Lai, B. (1986). *Nucl. Instrum. Methods*, A**246**, 337.
Chevalier, P. *et al.* (1995). *Nucl. Instrum. Methods*, A**354**, 584–587.
Engström, P., Fiedler, S. & Riekel, C. (1995). *Rev. Sci. Instrum.* In the press.
Engström, P., Larsson, S., Rindby, A., Buttkewitz, A., Garbe, S., Gaul, G., Knöchel, A. & Lechtenberg, F. (1991). *Nucl. Instrum. Methods*, A**302**, 547–552.
ESRF (1994). *Beamline Handbook*. ESRF, Grenoble, France.
Glover, I. D. & Helliwell, J. R. (1990). *Applications of Synchrotron Radiation*, edited by C. R. A. Catlow & G. N. Greaves, pp. 241–267. Glasgow: Blackie.
Hoffman, S. A., Thiel, D. J. & Bilderback, D. H. (1992). *Optics for High Brightness Synchrotron Radiation Beamlines*, Vol. 1740, edited by J. Arthur, pp. 252–257. San Diego: SPIE.
Høghøj, P., Joensen, K., Christensen, F. E., Susini, J., Ziegler, E., Freund, A. K., Lüken, E. & Riekel, C. (1994). *SPIE J.* **2011**, 354–359.

Høghøj, P., Ziegler, E. & Riekel, C. (1992). *d-Spacing Design of Double Multilayer X-ray Monochromator*. ESRF Report EXP/PH/92I01. ESRF, Grenoble, France.

Kaelble, E. F. (1967). Editor. *Handbook of X-rays*. New York: McGraw-Hill.

Moffat, K., Kuriyan, J., Gilbert, A., Ringe, D. & Karplus, M. (1986). *Structural Biological Applications of X-rays: Absorption, Scattering, and Diffraction*, edited by H. D. Bartunik & B. Chance, pp. 125–134. Orlando: Academic Press.

Pennartz, P. U., Löchner, U., Fuess, H. & Wroblewski, T. (1992). *J. Appl. Cryst.* **25**, 571–577.

Riekel, C. (1993). *SPIE J.* **1740**, 181–190.

Rosenbaum, G. & Holmes, K. C. (1980). *Synchrotron Radiation Research*, edited by H. Winick & S. Doniach, pp. 533–562. New York: Plenum Press.

Stephenson, G. B. (1988). *Nucl. Instrum. Methods*, A**266**, 447–451.

Thiel, D. J., Bilderback, D. H. & Lewis, A. (1992). *Optics for High Brightness Synchrotron Radiation Beamlines*, Vol. 1740, edited by J. Arthur, pp. 248–251. San Diego: SPIE.

Thompson, A. C. *et al.* (1992). *Nucl. Instrum. Methods*, A**319**, 320–325.

Underwood, J. H., Thompson, A. C., Wu, Y. & Giauque, R. D. (1988). *Nucl. Instrum. Methods*, A**266**, 296–302.

Wu, Y., Thompson, A. C., Underwood, J. H., Giauque, R. D., Chapman, K. L., Rivers, M. L. & Jones, K. W. (1990). *Nucl. Instrum. Methods*, A**291**, 146–151.

Ziegler, E., Marot, G., Freund, A. K., Joksch, St, Kawata, H., Berman, L. E. & Iarocci, M. (1992). *Rev. Sci. Instrum.* **63**, 496–500.